Direct Numerical Simulations of a Reacting Mixing Layer with Chemical Heat Release

P. A. McMurtry,* W.-H. Jou,† J. J. Riley,‡ and R. W. Metcalfe†
Flow Research Company, Kent, Washington

To study the coupling between chemical heat release and fluid dynamics, we have performed direct numerical simulations of a two-dimensional mixing layer undergoing a simple single-step chemical reaction with heat release. The reaction is a function only of the species concentrations and does not depend on temperature. We have treated the fully compressible equations, as well as an approximate set of equations that is asymptotically valid for low Mach number flows. These latter equations have the computational advantage that high-frequency acoustic waves have been filtered out, allowing much larger time steps to be taken in the numerical solution procedure. A derivation of these equations along with an outline of the numerical solution technique is given. Simulation results indicate that the rate of chemical product formed, the thickness of the mixing layer, and the amount of mass entrained into the layer all decrease with increasing rates of heat release. The vorticity dynamics are studied to analyze and interpret some effects of heat release on the fluid motion.

Nomenclature

C_i = molar concentration of ith chemical species
C_v = specific heat at constant volume
C_0 = uniform molar concentration of reactant in freestream
Ce = nondimensional heat release parameter
D_i = diffusivity of ith chemical species
Da = Damköhler number, $k_0 C_0 U_0 / L_0$
e = internal energy
ΔH = heat of reaction
k_0 = reaction rate constant
L_0 = wavelength of fundamental perturbation mode
M = Mach number
p = pressure
p^0 = thermodynamic pressure
p^1 = dynamic pressure
Pe = Peclet number, $D_0 / L_0 U_0$
Pr = Prandtl number, $\kappa / C_p \mu$
q = heat flux vector
$\dot{Q}$ = rate of heat release
R_i = rate of reaction of ith chemical species
Re = Reynolds number, $U_0 L_0 / \nu$
t = time
T = temperature
T_0 = initial freestream temperature
U_0 = velocity difference across mixing layer
v = velocity magnitude
$\boldsymbol{v}$ = velocity vector
$\boldsymbol{x}$ = position vector
γ = ratio of specific heats
ϵ = γM^2
κ = thermal conductivity
ρ = density
$\tilde{\tau}$ = stress tensor

Received Feb. 20, 1985; revision received Sept. 16, 1985. Copyright © American Institute of Aeronautics and Astronautics, Inc., 1985. All rights reserved.

*Graduate Student, Mechanical Engineering, University of Washington, Seattle, WA.
†Senior Research Scientist. Member AIAA.
‡Associate Professor, Mechanical Engineering, University of Washington, Seattle, WA. Member AIAA.

I. Introduction

THE development of accurate combustion models relies on understanding more fully the fundamental interactions among the thermal, chemical, and fluid dynamical processes in reacting flow systems. The work reported here is directed toward studying the interactions between chemical heat release and fluid dynamics, one of the least understood aspects of combustion. To achieve this purpose, we have performed direct numerical simulations of a two-dimensional, temporally growing mixing layer, including a single-step, irreversible chemical reaction between initially unmixed chemical species. The idea of direct numerical simulations is to use very accurate and efficient numerical methods to solve the governing equations for the detailed time evolution of the complex flowfield. The appeal of this method is that no closure modeling is necessary and the complete flowfield is known at every time step so that any statistical quantities of interest may be computed. The main disadvantage of this method is the limited range of spatial and temporal scales that can be resolved, restricting accurate numerical resolution to moderate Reynolds and Damköhler numbers. No turbulence or transport modeling has been attempted, limiting our study to the large-scale features of the fluid motion. However, the large-scale motions play a significant role in the evolution of a mixing layer and do not depend strongly on the Reynolds number.[1]

Previous direct numerical simulations of an incompressible reacting mixing layer without heat release[2] focused on how the turbulent flowfield affects the chemical reaction rates. This work has given physical insight into how the vortex roll-up and three-dimensional turbulence affect the chemical reaction. Furthermore, from comparisons of simulation results with laboratory data, this work has also led to increased confidence in the application of the direct numerical simulation methodology to this class of problems. However, because no heat release was allowed, the chemical reaction was a passive process and did not influence the fluid motion. In a reacting flow with heat release, the dynamics of the fluid motion are coupled with the chemical reaction through the nonhomogeneous density distribution caused by the thermal expansion. The work presented here attempts to include coupling between the chemical reaction, the heat release, and the flowfield.

To accomplish this goal, one may proceed to solve the compressible Navier-Stokes equation with heat production,

together with the species transport equations. This set of equations contains vorticity, entropy, and acoustic modes, a fact that can be established by analysis of the linearized equations.[3] In many practical cases, these modes are of greatly different frequencies. Particularly for low Mach number fluid motion, the acoustic modes are in frequency bands much higher than the other two modes. Therefore, in low Mach number flows, the acoustic fluctuations do not interact effectively with either the vorticity or entropy modes. From the computational point of view, tracking the acoustic fluctuations requires extremely small time steps, thus decreasing the efficiency of the computation as far as the vortex/entropy dynamics are concerned. Also, for very low Mach number flows, the round-off error can contaminate the calculation of the pressure gradient and the computed vortex motions can be significantly in error. For these reasons, we apply a set of approximate equations that is asymptotically valid for small Mach number flows. A discussion of these equations is given in Sec. II.

In Sec. III, a numerical solution procedure to solve the governing equations is outlined. The differences between the method used here and similar solution techniques for unsteady, constant-density flows are discussed.

Although a turbulent mixing layer is inherently three-dimensional, the two-dimensional simulations discussed here reveal important information about some of the dominant features. Laboratory experiments have shown that, at least in its early stages, the mixing layer is dominated by large-scale, two-dimensional vortices, with the growth of the layer dominated by the pairing of these vortices.[4] Two-dimensional simulations have been shown to accurately portray the characteristic large-scale roll-up and vortex pairing process of mixing layers.[5] The implications of heat-releasing chemistry on this process can thus be meaningfully addressed with two-dimensional simulations. In Sec. IV, simulation results with and without heat-releasing chemistry are presented. These results are analyzed to give some insight into the mechanisms responsible for the observed effects of heat release on the flow.

II. Low Mach Number Approximation

Detailed numerical solutions to general combustion processes are prohibited by excessive computer storage requirements and unacceptable computational expense. This results in part from the wide range of time and space scales present in reacting flow problems. For example, accurate resolution of the steep gradients of reacting species may require a grid spacing several orders of magnitude finer than that necessary to resolve other characteristic flow structures. Similarly, time scales characterizing acoustic wave propagation may be several orders of magnitude smaller than those characterizing convection processes. It is this last problem to which attention is directed here.

The existence of high-frequency acoustic waves places a severe restriction on the time-stepping increments used to numerically advance the fully compressible equations in time. To deal with this difficulty, an approximate set of equations valid for low Mach number flows is used. These equations have the computational advantage that acoustic waves have been filtered out, relieving the above-mentioned time-stepping constraint. However, at the same time they allow density nonuniformities resulting from heat release to develop. In the following, we have started from the exact governing equations. By using a small Mach number expansion, a set of ordered approximate equations is obtained. A set of criteria on other nondimensional parameters for the problem can also be obtained for the applicability of the approximation. This approach is essentially the same as employed by Sivashinsky[6] to study slow flame propagation in an enclosed volume and Rehm and Baum[7] in deriving approximate equations for buoyantly driven flows with slow heat addition. Application of similar equations in subsonic reacting flows has been discussed by Oran and Boris,[8] although the distinction between the lowest-order pressure and the first-order pressure was not discussed. This distinction is essential in both a theoretical framework and the numerical procedure.

Governing Equations

The conservation equations of mass, momentum, energy, and chemical species may be written in the following nondimensional form:

$$\frac{\partial \rho}{\partial t} + \nabla \cdot (\rho v) = 0 \tag{1a}$$

$$\gamma M^2 \rho \frac{\mathrm{D}v}{\mathrm{D}t} = -\nabla p + \frac{\gamma M^2}{Re} \nabla \cdot \bar{\tau} \tag{1b}$$

$$\rho \frac{\mathrm{D}}{\mathrm{D}t} E = -\nabla \cdot ((\gamma - 1) p v) - \frac{1}{PrRe} \nabla \cdot q + \frac{(\gamma - 1)\gamma M^2}{Re} (\nabla \cdot (\bar{\tau} \cdot v)) + DaCe\dot{Q} \tag{1c}$$

$$\frac{\partial C_i}{\partial t} + \nabla \cdot (C_i v) = DaR_i + \frac{1}{Pe} \nabla^2 C_i \tag{1d}$$

$$p = \rho T \tag{1e}$$

$$E = T + \tfrac{1}{2}\gamma(\gamma - 1) M^2 v^2$$

The velocity, density, temperature, and length are scaled by their respective reference quantities U_0, ρ_0, T_0, and L_0. The pressure is nondimensionalized by a reference thermodynamic pressure, $\rho_0 R T_0$ and time by L_0/U_0. The fluid is treated as a perfect gas and to simplify the computations the transport coefficients and specific heats are taken to be temperature independent constants. For a general discussion of the basic equations of combustion gas dynamics, see Williams.[9] To close this system of equations the following constitutive relations must be provided:

$$R_i = R_i(C_i, T), \qquad \dot{Q} = \dot{Q}(R_i)$$

$$q = q(\nabla T), \qquad \bar{\tau} = \bar{\tau}(\nabla v)$$

Pr, *Re*, *Da*, and *Pe* are the Prandtl, Reynolds, Damköhler, and Peclet numbers, respectively. *Ce* is a parameter specifying the amount of heat release and is given by $C_0 \Delta H \div \rho_0 C_v T_0$.

Small Mach Number Expansion

Defining $\epsilon = \gamma M^2$ and assuming that $\epsilon \ll 1$, the dependent variables may be expanded as power series in ϵ. Collecting the zero-order terms in ϵ results in the following lowest-order equations:

$$\frac{\partial p^{(0)}}{\partial t} + \nabla \cdot [\rho^{(0)} v^{(0)}] = 0 \tag{2a}$$

$$\nabla p^{(0)} = 0 \tag{2b}$$

$$\rho^{(0)} \frac{\mathrm{D}^{(0)}}{\mathrm{D}t} T^{(0)} = -(\gamma - 1) p^{(0)} \nabla \cdot v^{(0)} + \frac{1}{PrRe} \nabla \cdot q^{(0)} + DaCe\dot{Q} \tag{2c}$$

$$\frac{\partial C_i^{(0)}}{\partial t} + \nabla \cdot [C_i^{(0)} v^{(0)}] = DaR_i + \frac{1}{Pe} \nabla^2 C_i^{(0)} \tag{2d}$$

$$p^{(0)} = \rho^{(0)} T^{(0)} \tag{2e}$$

It is observed from this last set of equations that the momentum equation has been reduced to a description of the spatial variation of the thermodynamic pressure $p^{(0)}$. To complete the description of the velocity field, $v^{(0)}$, the first-order momentum equation must be included and is given as

$$\rho^{(0)}\frac{\mathrm{D}^{(0)}}{\mathrm{D}t}v^{(0)} = -\nabla p^{(1)} + \frac{1}{Re}\nabla\cdot\bar{\tau}^{(0)} \tag{2f}$$

It should be noted that all dependent variables appear only to lowest order except pressure; both $p^{(0)}$ and $p^{(1)}$ appear. The superscripts will now be dropped except to distinguish $p^{(0)}$ and $p^{(1)}$. The lowest-order momentum equation simply states that, in the first approximation, the thermodynamic pressure $p^{(0)}$ is constant in space but may vary with time. In this approximation, the sound speed is infinite so that any disturbances in thermodynamic pressure caused by combustion are felt instantaneously throughout the fluid. For combustion in an open domain, $p^{(0)} = p_\infty$, and the combustion is a constant-pressure process, a classical result of combustion analysis.[9] $p^{(1)}$ is the dynamic pressure associated with the fluid motion and, to the lowest order, does not participate directly in thermodynamic processes.

For the low Mach number approximation to remain valid, the parameter Ce must be restricted such that $DaCe \ll 1/M^2$. This can be seen from balancing terms in the energy equation (1c). If this restriction is not met, large velocities will be generated by the combustion and the assumption of low Mach number flow will not be valid.

These equations may be stated in an alternate form that proves to be helpful in obtaining numerical solutions. Equations (2a) and (2c) can be combined to give

$$\nabla\cdot v = \frac{1}{\gamma p^{(0)}}\left[\frac{\gamma\nabla\cdot q}{PrRe} - \frac{\mathrm{d}p^{(0)}}{\mathrm{d}t} + DaCe\dot{Q}\right] \tag{3}$$

In a closed domain with adiabatic walls or in a domain with periodic boundary conditions, Eq. (3) can be integrated to give

$$\frac{\mathrm{d}p^{(0)}}{\mathrm{d}t} = \frac{1}{\text{volume}}\iiint DaCe\dot{Q}\,\mathrm{d}V \tag{4}$$

Under these conditions the combustion is a constant-volume process, and the pressure in a closed domain increases due to the rate of chemical energy released in the chamber. Equations (3) and (4) are used to replace Eqs. (2b) and (2c), giving the final set of equations. Note that if the heat release term $\dot{Q}$ is zero and if heat conduction is negligible, then $\nabla\cdot v = 0$ and these equations reduce to those of a constant-density fluid.

III. Numerical Solution Procedure

The approximate equations are solved numerically using pseudospectral methods to compute spatial derivatives and a second-order Adams-Bashforth time-stepping scheme to advance the equations in time. The pseudospectral method involves expanding the dependent variables in a truncated series of smooth orthogonal functions that satisfy the boundary conditions (see Sec. IV). The velocity component transverse to the mean flow is expanded in a Fourier sine series and all other dependent variables are expanded in Fourier cosine series. Spatial derivatives are computed in Fourier space simply by differentiating the series term by term. Time advancement of the equations is done in physical space and fast Fourier transform routines are used to transform back and forth between physical and Fourier space. For details of the application of this numerical method, see Riley et al.[10] and Gottlieb and Orszag.[11] Numerical tests that were used to evaluate the performance of the computer code are presented in Ref. 10.

To solve the approximate equations, we first write Eqs. (2a) and (2f) in the following form:

$$\frac{\partial\rho}{\partial t} + \rho\nabla\cdot v + v\cdot\nabla\rho = 0 \tag{5}$$

$$\frac{\partial}{\partial t}(\rho v) = -\nabla p^{(1)} + A(x) \tag{6}$$

where $A(x)$ represents the viscous and convective components of the momentum equation. The local density is obtained by substituting Eq. (3) into Eq. (5) and advancing the density ahead in time using a second-order Adams-Bashforth time-stepping scheme. The chemical species equations are solved using the above-mentioned method in a straightforward manner.

The pressure and velocity components are obtained by solving Eq. (6) in two stages. First, Eq. (6) is advanced to an intermediate time step by neglecting the pressure effects,

$$\rho v^* = \rho v^n + \Delta t\left[\frac{3}{2}A(x)^n - \frac{1}{2}A(x)^{n-1}\right] \tag{7}$$

The remaining pressure term gives

$$\frac{(\rho v)^{n+1} - (\rho v)^*}{\Delta t} = -\nabla p^{(1)^{n+1/2}} \tag{8}$$

Note that adding Eqs. (7) and (8) results in a second-order accurate finite difference approximation to the time derivative of ρv. Taking the divergence of Eq. (8) gives the following Poisson equation for pressure:

$$-\nabla^2[p^{(1)^{n+1/2}}] = \frac{\nabla\cdot(\rho v)^{n+1} - \nabla\cdot(\rho v)^*}{\Delta t} \tag{9}$$

Since we are treating a spatially periodic problem in this work (see Sec. IV), Eq. (9) is easily solved for $p^{(1)}$ by taking the Fourier transform of the equation, solving for the transform of $p^{(1)}$, and then transforming back to physical space. The velocity components are obtained by using this value of $p^{(1)}$ in Eq. (8). This method is similar to numerical solution techniques for the constant-density, unsteady, Navier-Stokes equations as outlined by Peyret and Taylor.[12] The important difference is that the density is not constant, and an approximation for $\nabla\cdot(\rho v)^{n+1}$ must be obtained directly from the continuity equation. Computed values of ρ^{n+1}, ρ^n, and ρ^{n-1} are used to obtain a second-order accurate estimate to $\partial\rho^{n+1}/\partial t$, giving $-\nabla\cdot(\rho v)^{n+1}$ from Eq. (2a).

IV. Simulation Results

In this section, we discuss results of our numerical simulations of the temporal development of a chemically reacting mixing layer with heat release. The computational domain is a rectangle with 64×64 equally spaced grid points. The flow is assumed periodic in the streamwise direction and free-slip, impermeable boundary conditions are employed at the transverse boundary. The initialization of the flowfield is the same as used by Riley and Metcalfe[2] in their two-dimensional simulations of a constant-density reacting mixing layer. Namely, the velocity field was initialized with a hyperbolic tangent profile added to perturbations corresponding to the most unstable mode and its subharmonic as determined from linear stability theory.[13] The chemical reactant concentrations were set as follows:

$$C_1(x,0) = \frac{1}{y_0\sqrt{\pi}}\int_\infty^y \exp(-\zeta^2/y_0^2)\mathrm{d}\zeta$$

$$C_2(x,0) = 1 - C_1$$

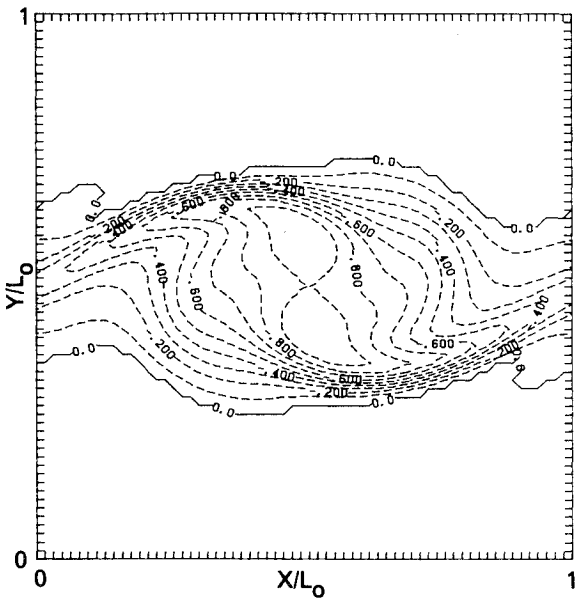

a) Low Mach number approximation, $t=8$.

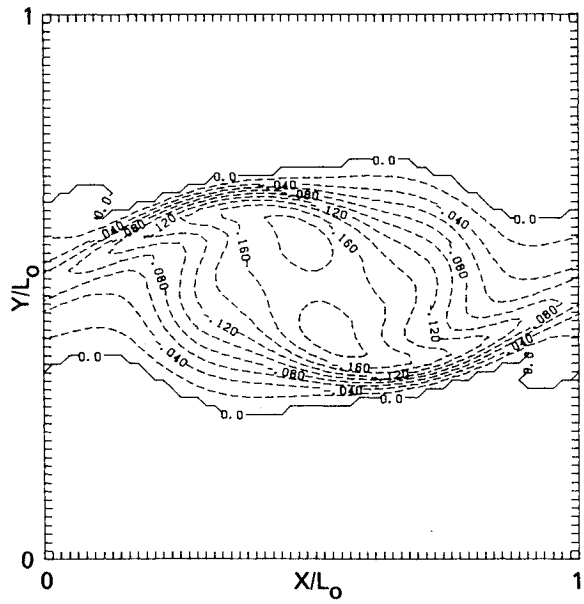

b) Fully compressible calculation, $t=8$ (contours scaled by $M=0.2$).

Fig. 1 Vorticity contours comparing simulation results for the low Mach number approximation and the exact, fully compressible equations of motion ($Ce=2.0$).

The combustion is a constant-volume process and the chemical reaction studied here is a single-step, irreversible reaction,

$$C_1 + C_2 \rightarrow \text{product} + \text{heat}$$

The reaction rate is taken to be a function of only the reactant concentrations and is not temperature dependent.

All simulations were performed at a Reynolds number of 250, a Peclet number of 100, and a Damköhler number of 1.5. Using the low Mach number approximation, three different cases have been computed for different values of the heat release parameter Ce in order to study its effects on the flow.

With these parameter values, the fluid motion on the computational grid is accurately resolved. The values of the

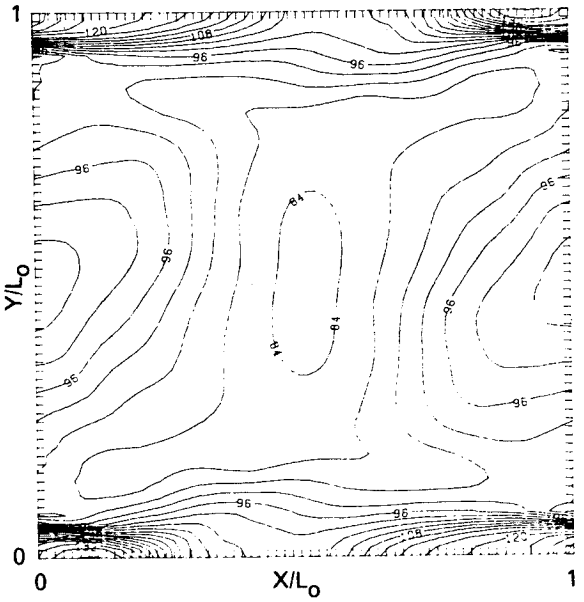

Fig. 2 Pressure contours obtained from the fully compressible equations of motion ($t=8$).

Reynolds and Damköhler numbers are considerably lower than in related laboratory experiments. In the experiments performed by Hermanson et al.,[14] the Reynolds number was 7000 (based on velocity layer thickness) and the Damköhler number was 25-125 (based on the local large-scale characteristic time, L_0/U_0). The difference in Reynolds number is not important for quantities that depend on the large-scale structures of the flow.[5] However, the rate of chemical reaction depends critically on the small-scale, three-dimensional turbulence and the difference in Reynolds number could be important for these effects. The lower value of the Damköhler number along with a temperature-independent reaction is necessary to accurately resolve the gradients of the reacting species concentrations that occur across the reaction front. As a result, the reaction zone in these simulations is thicker than most nonpremixed diffusion reactions of interest. Although we lose some important physical features of real reacting flows with these simplifications, we are able to study details of the effects of heat release on the large-scale mixing and vorticity dynamics of reacting flows.

The validity of the low Mach number approximation in the parameter range of the simulations discussed here has been tested by solving the exact, fully compressible equations (1a-1f) for a reacting mixing layer with a Mach number of 0.2. Only a single roll-up of the fundamental mode was computed because of the excessive computational costs associated with the solution of the fully compressible equations. Vorticity contours obtained from solutions of the exact and approximate equations are compared in Fig. 1. Although acoustic waves propagate throughout the flowfield, they apparently have no influence on the vorticity dynamics. The pressure field, plotted in Fig. 2, shows the evidence of acoustic waves. These acoustic waves have a frequency much greater than the hydrodynamic frequency, so that, as mentioned earlier, the hydrodynamics cannot respond to the acoustic fluctuations.

Figures 3 and 4 are contour plots of the product concentration in the reacting mixing layer obtained from two different simulations, the only difference being the amount of heat released ($Ce=0$ and 5), all other parameters being equal. The development of the layer into the now widely recognized large coherent structures and the pairing process of these structures is clearly evident. The main difference observed in these two cases is the amount of chemical prod-

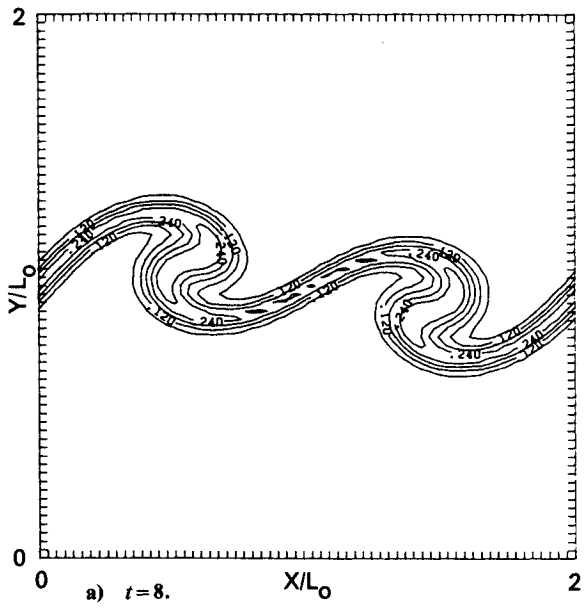

a) $t=8.$

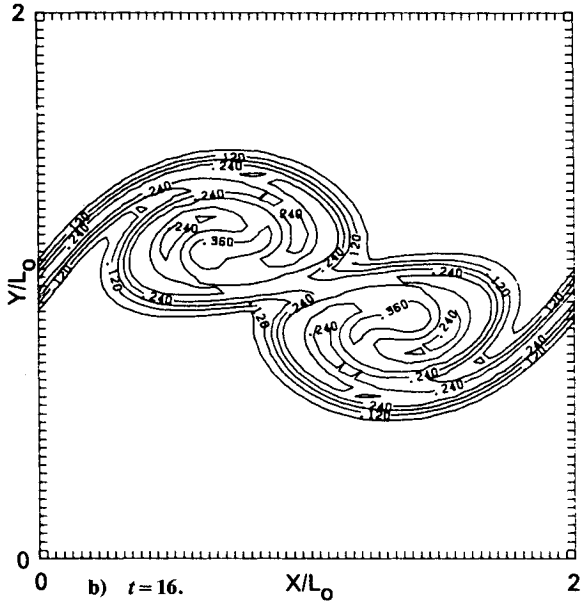

b) $t=16.$

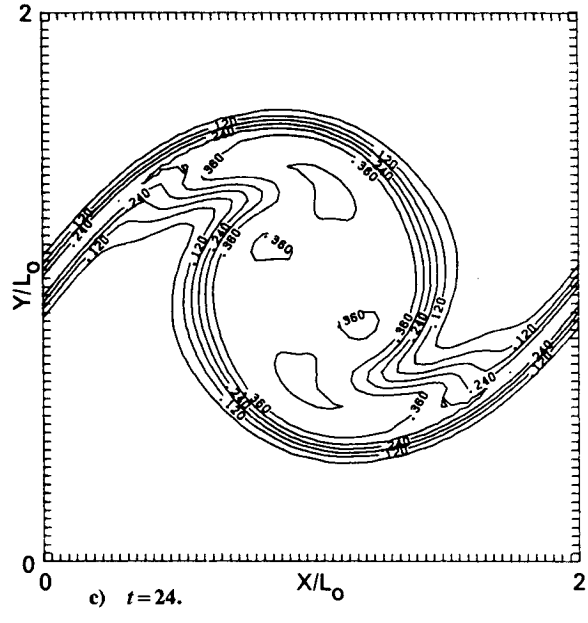

c) $t=24.$

Fig. 3 Chemical product contour plots, no heat release ($Ce=0$).

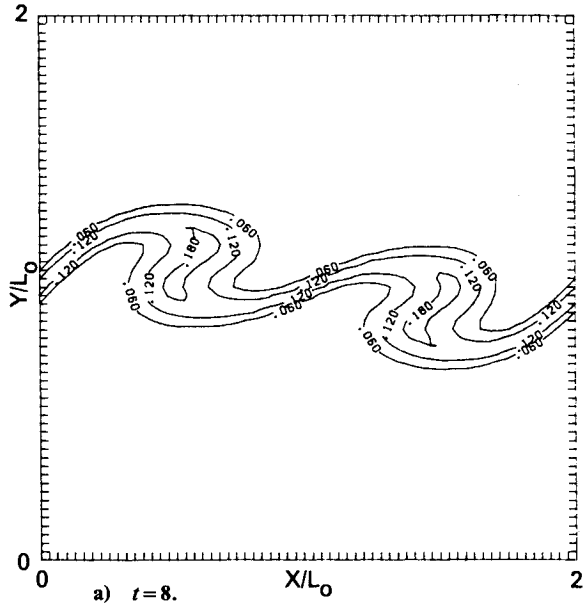

a) $t=8.$

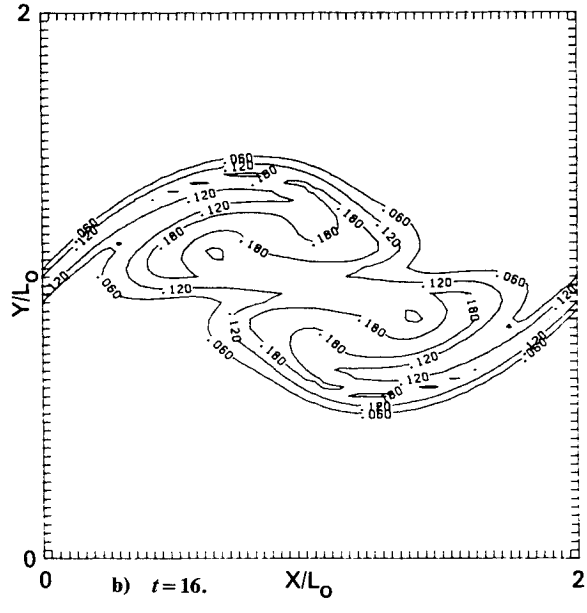

b) $t=16.$

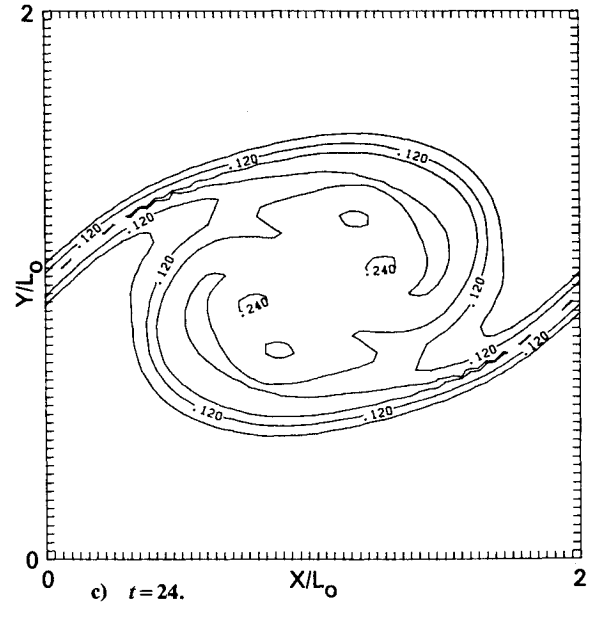

c) $t=24.$

Fig. 4 Chemical product contour plots, with heat release ($Ce=5$).

uct formed, with the effect of heat release being to significantly reduce the rate of product generation in the layer. Concentration profiles averaged horizontally across the layer are shown in Fig. 5 for all three simulations, indicating the reduction in product as the heat release increases. For more realistic temperature-dependent reactions, we can envision that the expected increase in reaction rate with increasing temperature (heat release) will be partially offset by the reduced density and mass entrainment in the vortices. Averaged temperature profiles are displayed in Fig. 6. The thickness of the layer, based on the point at which either the average product or temperature approaches freestream values, is seen to remain approximately the same, with a possible slight decrease indicated.

A plot of the velocity deficit in a mixing layer with and without heat release (Fig. 7) gives another indication that the layer thickness decreases with increasing heat release. Computed velocity profiles in Fig. 8 show a steeper maximum slope for the heat release computations, confirming the reduced growth rate of a mixing layer with chemical heat release. Because of the decrease in density caused by exothermic chemical reactions and since the overall layer growth rate is slower, the heat release must act to decrease the rate of mass entrainment into the layer. These results are in qualitative agreement with the experimental findings of Wallace[15] and Hermanson et al.,[14] who conducted experimental studies of mixing layers that included chemical reactions with varying degrees of heat release.

To explain these results, it is useful to study the flowfield in terms of the vorticity dynamics and to observe how the heat release affects the vorticity field. For a two-dimensional mixing layer, the vorticity equation may be written as

$$\frac{D\omega}{Dt}+\omega\nabla\cdot v=\frac{1}{\rho^2}(\nabla\rho\times\nabla p)+\frac{1}{Re}\nabla\times(\nabla\cdot\bar{\tau})$$

The first term on the right-hand side is referred to as the baroclinic torque and the second term on the left-hand side represents a change in vorticity resulting from thermal expansion. If there are no heat sources present in the flow ($\nabla\cdot v=0$) and $\rho=$ const so that aside from diffusion effects, vorticity is conserved along particle paths. Figure 9 shows the vorticity contours at times of $t=8$, 16, and 24 for a reacting mixing layer without heat release. The vorticity is of

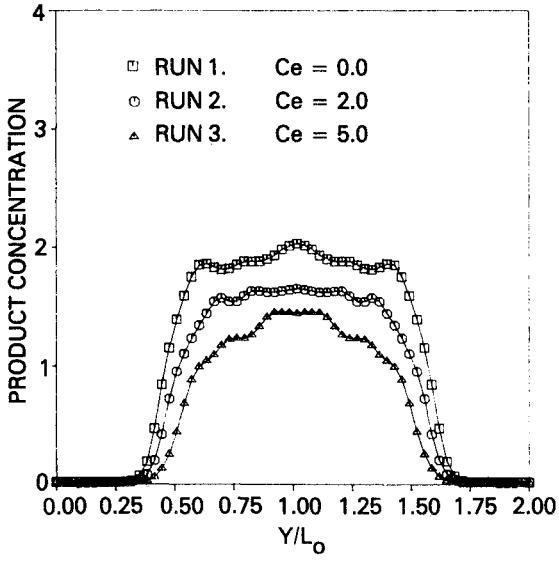

Fig. 5 Average product concentration across mixing layer ($t=24$).

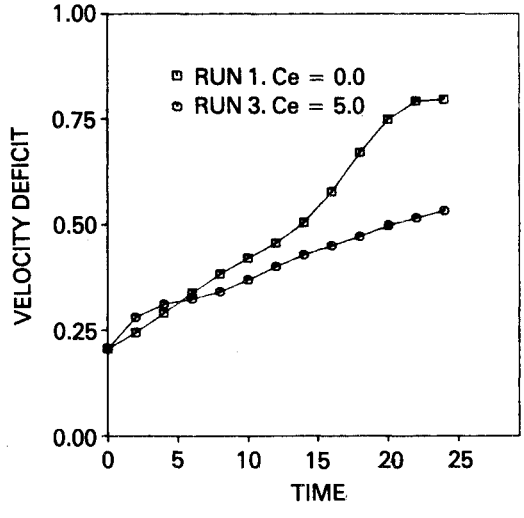

Fig. 7 Integrated velocity deficit vs time.

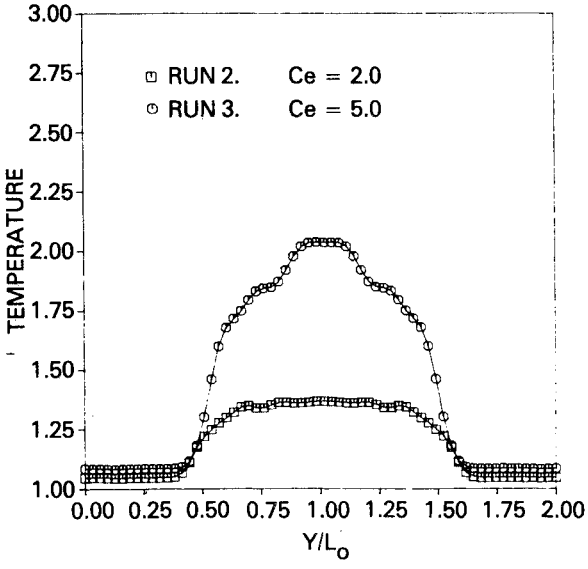

Fig. 6 Average temperature profile across mixing layer ($t=24$).

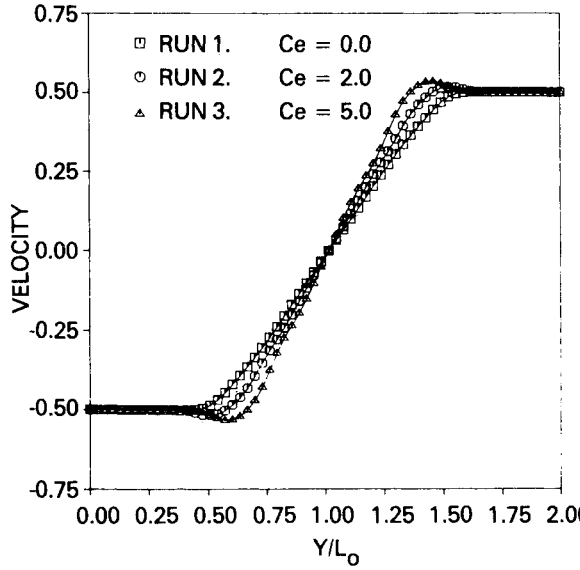

Fig. 8 Velocity profile across mixing layer ($t=24$).

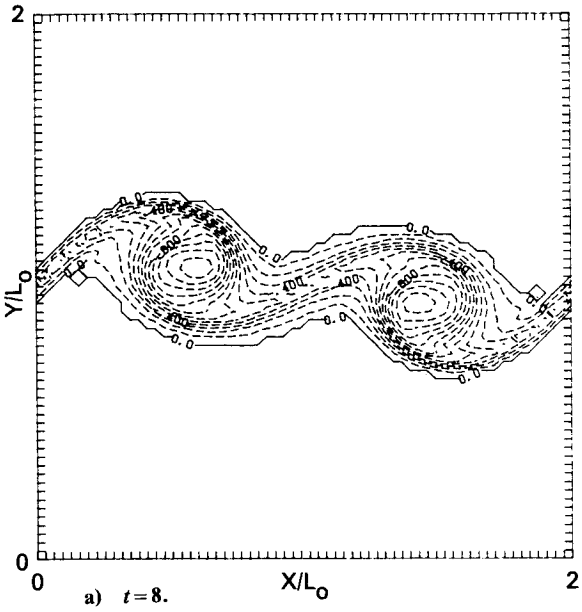

a) $t=8.$

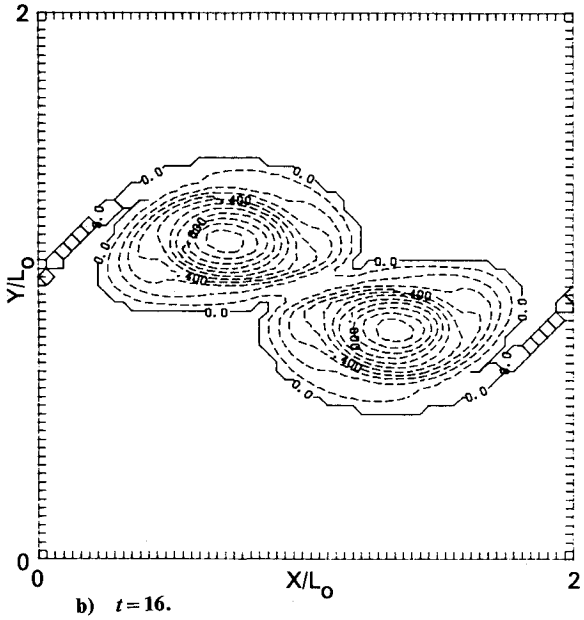

b) $t=16.$

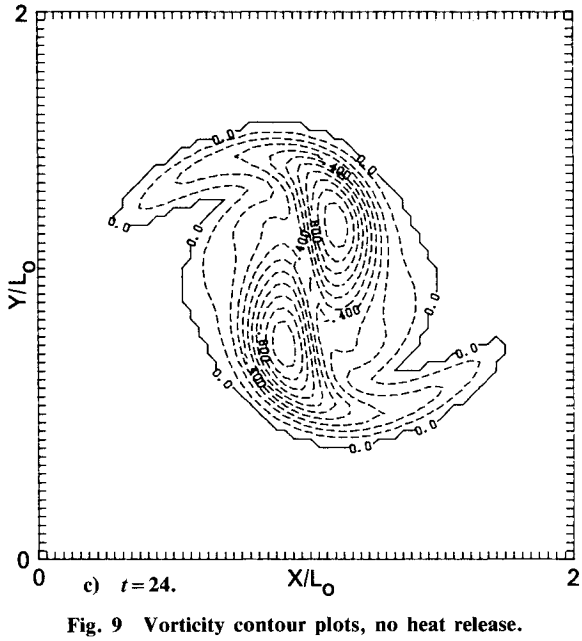

c) $t=24.$

Fig. 9 Vorticity contour plots, no heat release.

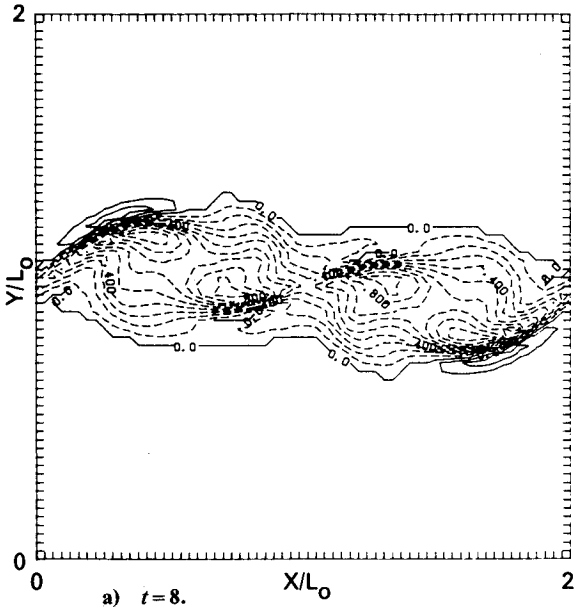

a) $t=8.$

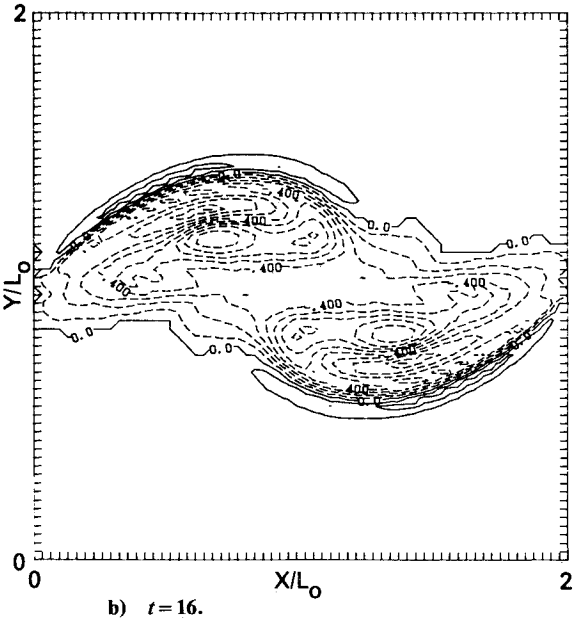

b) $t=16.$

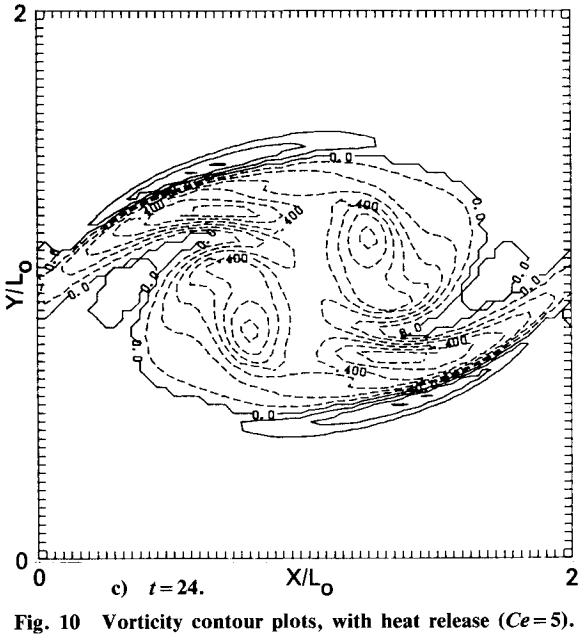

c) $t=24.$

Fig. 10 Vorticity contour plots, with heat release ($Ce=5$).

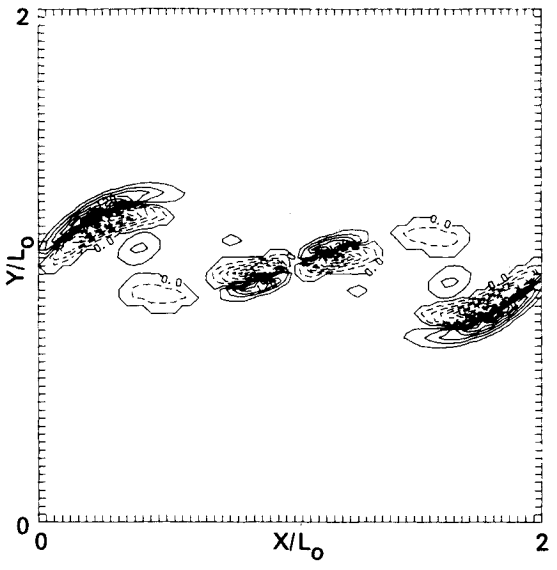

a) $t=8$.

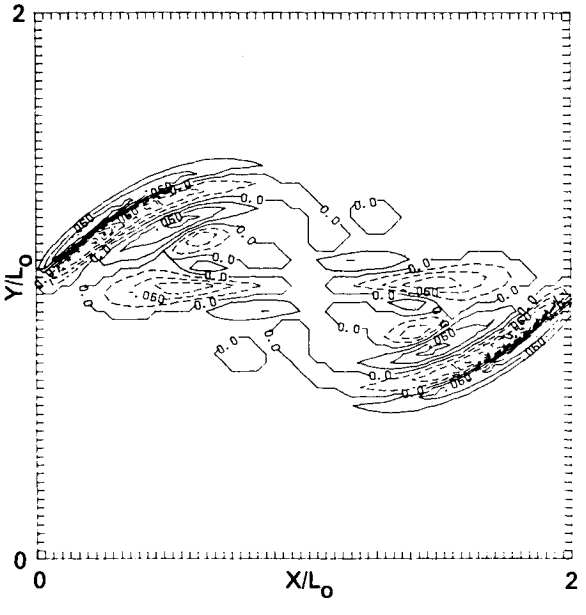

b) $t=16$.

Fig. 11 Baroclinic torque ($Ce=5$).

the same sign throughout the flowfield and the large-scale structures of the flow are clearly apparent. The vorticity field for a mixing layer with heat release (run 3, $Ce=5$) is shown in Fig. 10.

An important effect of heat release on the vorticity field has been to decrease the vorticity at the center of the vortex structures. This is a result of thermal expansion in the vortex cores, which is most pronounced at early times since low-density combustion products are rapidly formed in the vortex cores. Because the total vorticity is conserved (the circulation around the computational domain can easily be proved to remain constant in these simulations), this will result in a more diffuse vorticity field than in the no heat release case.

The heat release has also caused the vorticity field to take on a much less structured appearance compared with the no heat release case, and multiple local extrema in the vorticity field have developed. This latter observation appears to be a result of the baroclinic torque and also contributes to a more diffuse vorticity distribution. The result of a more diffuse vorticity field will be to reduce the vertical velocity component of the fluid, thus reducing the straining of the reaction interface and the mass entrainment, and hence decreasing the overall chemical reaction.

The instantaneous action of the baroclinic torque at times of $t=8$ and 16 is shown in Fig. 11. A qualitative explanation for these complicated-looking plots is as follows. The direction of the pressure gradient is roughly radially outward from the center of the vortex structures and is monotonic across the reaction front. However, the density gradient changes sign across the reaction front, resulting in a change in sign of the baroclinic torque in the reaction zone. As the layer rolls up, the reaction zone becomes highly distorted, and the complicated structure of the baroclinic torque shown in Fig. 11 results.¶ The change in sign of vorticity across the reaction zone results in the generation of vorticity that alternately opposes and enhances the vorticity field in neighboring regions and in the appearance of local extrema in the vorticity. The baroclinic torque has also resulted in the generation of a region of positive-signed vorticity at the outer edges of the layer. This indicates a change in sign of the velocity gradient, explaining the inflection point in the velocity profile seen in Fig. 8.

Because our simulations have been limited to two spatial dimensions, some potentially important physics have been lost. For example, vortex stretching, an inherently three-dimensional phenomenon, cannot be represented and may be a significant part of the overall vorticity dynamics. The influence of the baroclinic torque on the vorticity dynamics may, on the other hand, be less apparent in full three-dimensional calculations.

Another effect of heat release in reacting flows will generally be to raise the viscosity, thus lowering the Reynolds number. It can be argued that this will tend to have a stabilizing effect on the flow. If the Reynolds number is large enough, the dynamics of the mixing layer do not, however, depend strongly on the Reynolds number. In the simulations presented here, the viscosity has been held constant. In other flow configurations, where the instability or other important features of the flow are more dependent on Reynolds number (for example, boundary-layer flows), ignoring Reynolds number dependence could give quite misleading results.

All simulations were performed on the NASA Lewis Cray-1. Computation times were approximately 0.20 s per time step on a 64×64 computational grid. The simulations presented here were carried out 1200 time steps.

V. Conclusions

The application of the approximate set of equations derived here for low Mach number flows has resulted in a significant reduction in computer costs compared with solutions to the exact, fully compressible equations of motion. The computing time needed to integrate the governing equations has been reduced by a factor of approximately $1/M$ using the low Mach number approximation. Excellent agreement with the exact equations has been obtained for the cases presented here.

Simulation results in two spatial dimensions of a chemically reacting mixing layer indicate that the amount of mass entrained into the layer is reduced as the rate of heat release increases. The thickness of the layer is also reduced when exothermic chemical reactions occur. These results are in qualitative agreement with recent mixing layer experiments that have included chemical reactions with heat release.

These simulations demonstrate the effectiveness of the direct numerical simulation approach as a predictive tool in studying complex reacting flows with heat release. An extension of this work to three spatial dimensions should provide

¶This qualitative picture benefited from a discussion with Prof. F. A. Williams of Princeton University.

insight into the more complex problem of the interactions between turbulence and heat release in reacting flows.

Acknowledgment

This work has been sponsored by NASA Lewis Research Center under Contract NAS3-24229.

References

[1]Roshko, A., "Structures of Turbulent Shear Flows: A New Look," *AIAA Journal*, Vol. 14, 1976, pp. 1349-1357.

[2]Riley, J. J. and Metcalfe, R. W., "Direct Simulations of Chemically Reacting Turbulent Mixing Layers," NASA CR 17460, 1984.

[3]Chu, B.-T. and Kovasznay, L.S.G., "Nonlinear Interactions in a Viscous Heat-Conducting Compressible Gas," *Journal of Fluid Mechanics*, Vol. 3, 1958, pp. 494-514.

[4]Winant, C. D. and Browand, F. K., "Vortex Pairing, the Mechanism of Turbulent Mixing-Layer Growth at Moderate Reynolds Number," *Journal of Fluid Mechanics*, Vol. 63, 1974, pp. 237-255.

[5]Riley, J. J. and Metcalfe, R. W., "Direct Numerical Simulation of a Perturbed, Turbulent Mixing Layer," AIAA Paper 80-0274, Jan. 1980.

[6]Sivashinsky, G. J., "Hydrodynamic Theory of Flame Propagation in an Enclosed Volume," *Acta Astronautica*, Vol. 6, 1979, pp. 631-645.

[7]Rehm, R. G. and Baum, H. R., "The Equations of Motion for Thermally Driven, Buoyant Flows," *Journal of Research of the National Bureau of Standards*, Vol. 83, 1978, pp. 297-308.

[8]Oran, E. S. and Boris, J. P., "Detailed Modelling of Combustion Systems," *Progress in Energy and Combustion Science*, Vol. 7, 1981, pp. 1-72.

[9]Williams, F. A., *Combustion Theory*, Addison-Wesley, Reading, MA, 1965.

[10]Riley, J. J., Metcalfe, R. W., and Orszag, S. A., "Direct Numerical Simulations of Chemically Reacting Turbulent Mixing Layers," *The Physics of Fluids*, Vol. 25, 1986, pp. 406-422.

[11]Gottlieb, D. and Orszag, S. A., *Numerical Analysis of Spectral Methods*, SIAM, 1977.

[12]Peyret, R. and Taylor, T. D., *Computational Methods for Fluid Flow*, Springer-Verlag, New York, 1983, pp. 160-169.

[13]Michalke, A., "On the Inviscid Instability of the Hyperbolic Tangent Velocity Profile," *Journal of Fluid Mechanics*, Vol. 19, 1964, pp. 543-556.

[14]Hermanson, J. C., Mungal, M. G., and Dimotakis, P. E., "Heat Release Effects on Shear Layer Growth and Entrainment," AIAA Paper 85-0142, Jan. 1985.

[15]Wallace, A. K., "Experimental Investigation on the Effects of Chemical Heat Release in the Reacting Turbulent Plane Shear Layer," Ph.D. Thesis, University of Adelaide, Australia, 1981.

From the AIAA Progress in Astronautics and Aeronautics Series . . .

VISCOUS FLOW DRAG REDUCTION—v. 72

Edited by Gary R. Hough, Vought Advanced Technology Center

One of the most important goals of modern fluid dynamics is the achievement of high speed flight with the least possible expenditure of fuel. Under today's conditions of high fuel costs, the emphasis on energy conservation and on fuel economy has become especially important in civil air transportation. An important path toward these goals lies in the direction of drag reduction, the theme of this book. Historically, the reduction of drag has been achieved by means of better understanding and better control of the boundary layer, including the separation region and the wake of the body. In recent years it has become apparent that, together with the fluid-mechanical approach, it is important to understand the physics of fluids at the smallest dimensions, in fact, at the molecular level. More and more, physicists are joining with fluid dynamicists in the quest for understanding of such phenomena as the origins of turbulence and the nature of fluid-surface interaction. In the field of underwater motion, this has led to extensive study of the role of high molecular weight additives in reducing skin friction and in controlling boundary layer transition, with beneficial effects on the drag of submerged bodies. This entire range of topics is covered by the papers in this volume, offering the aerodynamicist and the hydrodynamicist new basic knowledge of the phenomena to be mastered in order to reduce the drag of a vehicle.

Published in 1980,456 pp., 6×9, illus., $35.00 Mem., $65.00 List

TO ORDER WRITE: Publications Order Dept., AIAA, 1633 Broadway, New York, N.Y. 10019